https://doi.org/10.1016/j.solmat.2020.110693

Cost-effective and Eco-friendly Laser-processed Cotton Paper for High-performance Solar Evaporation

Y.L. Wang, G.J. Li, K.C. Chan*

Advanced Manufacturing Technology Research Centre, Department of Industrial and Systems Engineering, The Hong Kong Polytechnic University, Hung Hom, Kowloon, Hong Kong

* Corresponding author. E-mail address: kc.chan@polyu.edu.hk (K.C. Chan).

Abstract

Recently, interfacial solar-driven evaporation has received tremendous attention due to its potential for enhancing solar thermal conversation ability via heat localization at the evaporation interface. Diverse materials and configurations have been explored to boost the evaporation using plastic foam as the thermal insulator at the cost of complex assembly and environmental threats. Herein, we demonstrate a biodegradable, cost-effective, and scalable three-dimensional (3D) cotton paper-based solar steam generator prepared by one-step laser-induced forward transfer in the ambient atmosphere. The as-prepared evaporator has excellent solar absorption ability. The defining advantages of this method are that it can easily form a 3D structure and it is free from hazardous raw material involvement and waste generation. With further novel design by using a natural air gap instead of artificial plastic material to insulate the steam generation area and the underlying bulk water, the as-prepared evaporation system can achieve a high evaporation rate of 1711 g m^{-2} h^{-1} with a corresponding efficiency of 83% under one sun illumination. Such solar vaporization functions offer new insights into the future development of high-performance solar steam generators through an environmentally friendly and cost-effective pathway.

Keywords: Photothermal conversion; Interfacial water evaporation; Laser-induced forward transfer

1. Introduction

Social development hindrances due to freshwater scarcity are becoming increasingly worthy of attention. The annual solar radiation energy is equivalent to 1000 times the energy consumed by the entire human population during the same period [1]. As a facile and effective technology for seawater desalination, solar-driven water purification technology has attracted tremendous attention in recent years. High-efficiency solar evaporation can provide a new possibility for off-grid sterilization, domestic heating in coastal areas, electricity generation, and sewage treatment apart from seawater desalination [2-4].

In the early development stage of solar evaporation, the limited freshwater separation rate induced by the poor light absorption ability and the non-negligible heat loss makes it not sufficient to fulfill the daily demands of human [5-7]. Among various emerging photoabsorbing materials, plasmonic nanoparticles [8-10], semiconductors [11-13], and diverse carbon-based materials [14, 15] have been extensively investigated for achieving near full broadband solar absorption. Due to their high material cost or complicated fabrication processes, it is still challenging to use them for large scale applications. As shown in Table 1 [16], the durable metallic nanoparticles are mainly pricey noble metal material (Au [17], Pd [18]), limiting their mass production. Semiconductors with narrow bandgaps, such as TiO_x ($x<2$) nanoparticles [19], can offer an impressive wide-spectrum absorption ability. Nevertheless, the large-scale implantation value of such material is heavily degraded due to the extensive use of costly magnesium as a reducing agent. The emerging achievements of carbon materials seem to provide a new possibility in developing inexpensive solar generators, challenges remain in terms of tedious synthesis process [20], and high-temperature annealing treatment [21], which will also limit their practical use. It is thus essential to develop a solar steam generator with systematic considerations of high photothermal ability, low cost, and high environmental friendliness.

Table 1. Solar evaporation efficiency and material cost photothermal materials [16]

Type of materials	Work	Solar evaporation Efficiency (%)	Unit cost US$ per gram	Scalability	Reference
Plasmonic metals	AuNR/AuNS/paper	87	384	Yes	[17]
	Pd NPs/wood	85	1394	Yes	[18]
Semiconductors	Black TiOx coated stainless steel mesh	50	5.47	No	[19]

	Black titania film	70	5.47	No	[22]
Diverse carbon materials	Exfoliated graphite/carbon foam	85	1.9	Yes	[5]
	rGO/BNC	83	580	No	[20]
	GO film on cellulose wrapped polystyrene foam	80	122	Yes	[23]
	Graphene foil supported porous graphene sponge	89.6	602	Yes	[24]

Apart from limited light absorption ability, thermal conduction to underlying seawater accounts for the main reason for low light-to-vapor conversion efficiency in solar evaporation. By avoiding heating the entire evaporation system and sacrificing solar energy, methods of localizing heat at the evaporation interface have been widely considered as effective measures to enhance the photothermal conversion efficiency [25, 26]. In recently reported works, plastic foam with low thermal conductivity (~0.04 W m^{-1} K^{-1}) is commonly used as the thermal separators between photoabsorber materials and seawater to suppress heat conduction loss [6, 27, 28]. For the first demonstration of this approach, insulated and hydrophilic carbon foam was used by Ghasemi et al. [5] to achieve heat localization. These structural characteristics helped achieve solar thermal efficiency up to 85% at 10 kW m^{-2}. After that, some interfacial solar vapor generators can realize high solar-vapor efficiencies approaching 60%-87% at 1000 W m^{-2} [29-31]. Recently, the hierarchical Ti foams/PU sponge evaporator reported by Yin et al. [32] could even achieve extremely high water evaporation efficiency of 90%. Nevertheless, the assembly process is labor-intensive and limited to lab-scale production. The large difference in hydrophilicity of the high-cost light absorbers and physical insulators makes the whole devices suffer from a high risk of detachment on a natural fluctuating water surface. The suppressed water supply highly impairs the evaporation rate. Under this condition, the evaporator prone to be overheated under long-term illumination, especially in the edge areas where the heat exchange with the surrounding environment is rapid, which in turn further inhibits evaporation. Designing and fabricating eco-friendly solar absorbers that have a strong water pumping and storage capacity in themselves is therefore important. Furthermore, chemical material consumption, complicated assembly processes, and plastic pollution remain as challenges for a greener development of solar interfacial evaporation devices.

Herein, we demonstrate an innovative design of a three-dimensional (3D) cotton paper-based porous evaporator that operates above the water surface, taking advantage of the natural air gap as a thermal insulator to the underlying cold water. The one-step laser printing method is used to transfer laser-induced graphene on the surface of cotton

paper to harness the solar flux directly in the ambient environment [33-35]. The selection of cotton paper as the substrate for the fabrication of 3D evaporator is critical. As a cost-effective, flexible, and biodegradable agricultural product, cotton has excellent water absorption properties and extremely low thermal conductivity (~0.035 W m^{-1} K^{-1}) [14]. Wet multilayer cotton paper with mesoporous fibers can form an interconnected open 3D structure, which significantly amplifies the effective evaporation surface. Additionally, since the entire evaporator is designed to be located above the water surface instead of floating on it, the air gap formed can serve as an insulator to reduce heat loss. In the usual room temperature environment (25 ℃, RH 45%), air enjoys a low thermal conductivity (0.025 W m^{-1} k^{-1}), and only 4.3% of that of water [36]. Although the thermal conductivity of air slightly increases with increasing temperature, this advantage is still considerable. Even in an extreme environment of 100 ℃, which is difficult to reach for most solar evaporators during operation, the thermal conductivity of the humid air is only 0.032 W m^{-1} k^{-1}.

2. Experimental section

2.1. Materials and fabrication of 3D laser-printed evaporator

A commercial polyimide film of thickness 0.05 mm was used for subsequent laser processing without pretreatment. The cotton paper substrate was supplied by Mannings Commercial Chain Co., Ltd. The 1064 nm laser source (DMG Lasertec 40) for the 3D printing process was fixed at 3 W with a scanning rate of 400 mm s−1 in an ambient environment. Taking advantage of the laser-induced forward transfer method [33, 34], graphene was deposited on the surface of cotton paper underneath the polyimide film. The resultant light trapping paper was laminated with layers of untreated substrate paper to form a 3D evaporation structure.

2.2. Steam generation and outdoor desalination test

The steam generation experiments were conducted at ambient temperature and humidity of around 23 °C and 58%, respectively. A calibrated Newport solar simulator (LCS-100 94011A) was used to provide constant one sun illumination (1000 W m^{-2}). Real-time detection and recording of the mass changes were performed on an analytical balance (Mettler Toledo MS205DU) connected to a computer via RS 232 serial ports. K-type thermocouples were

used to monitor the temperature distribution of the entire system. Both the temperature and humidity of the air gap layer under steady-state were measured by a high precision temperature and humidity meter (Victor 231).

2.3. Measurement and characterization

A LabRAM HR 800 Raman spectrometer with a laser source of 488 nm was used to collect the Raman spectra of the as-printed graphene on cotton paper. The SEM images and optical spectra of both the pristine cotton paper and laser synthesized light-absorbing paper were characterized. The absorbance efficiency A (%) can be obtained through the formula: A=1-T-R, where the transmittance and reflectance efficiency are represented by T (%) and R (%), respectively. Thus, the optical absorption ability across the full solar spectrum can be calculated by the formula $A_{full} = \frac{\int A \cdot I d\lambda}{\int I d\lambda}$. Here, I (W m^2) is irradiance and λ (nm) is the wavelength based on the air mass 1.5 global (AM 1.5 G) irradiation spectra.

3. Result and discussion

The configuration and additive manufacturing process of the cotton paper-based evaporator are schematically illustrated in Fig. 1. Interfacial vapor generation that localizes photothermal conversion to the water/air interface is an effective method to reduce heat loss. As the configuration shows in Fig. 1a, the insulated foam has been widely used as floating support for interfacial evaporation. However, as discussed above, this method suffers from a high risk of detachment, overheating in the central area of the evaporator, and plastic pollution. In this work, we first demonstrate the method by taking advantage of a natural air gap for thermal insulation illustrated in Fig. 1b. Fig. 1c presents the process of laser-induced graphene transfer. The polyimide film was directly placed above cotton paper so that the laser-generated graphene could be deposited on the cotton paper as photoabsorbers in an ambient atmosphere (Fig. S1). A small power (5 W) laser post-treatment was conducted to provide an annealing effect and to make sure the generated graphene and cotton paper substrate were closely integrated. At the same time, it enhances hydrophilicity by further shortening the cotton fibers and creating more defects on the transferred graphene flakes. Here, the untreated cotton paper severs as wicking material to ensure a sufficient and continuous supply of water to all the 3D evaporation sites (Fig. 1d). 12 cm^2 of cotton paper can reach water saturation within 130 s (Fig. S2). By calculating the weight

gain of the cotton paper after being fully wetted by pure water, the water absorption rate was found to be as high as 29 kg m^{-2} h^{-1}, which is almost ten times the current interfacial evaporation data published in the related literature. Pristine cotton paper is not adequate for the high absorption of broadband wavelength light. As shown in the optical spectrum (Fig. 2a), the as-printed cotton paper enjoys a high absorptance of 0.98, indicating a unique opportunity for developing effective photoabsorbers. The chemical composition of the transferred graphene was characterized by the Raman spectrum, as shown in Fig. 2b. The G peak and the 2D peak was at 1580 cm^{-1} and 2700 cm^{-1}, respectively. The D peak at 1350 cm^{-1} was contributed by the sp^2 bonds of the graphene flakes with disordered orientation. SEM images (Fig. 3a-d) revealed the microscopic structures of both the pristine and the laser-treated cotton paper. The pristine cotton paper shows a 3D porous and loose structure formed by randomly connected long and thin fibers (Fig. 3a), with relatively smooth and compact surfaces (Fig. 3b). After the laser transfer process, layers of fuzzy graphene flakes deposited on the surface of cotton paper can be observed as in Fig. 3c. Due to the instantaneous high heat of the laser, the fibers were significantly shortened and roughened. With zoom-in observation (Fig. 3d), extensive randomly distributed micro-sized pores can be observed among the deposited graphene, which act as channels for both water delivery and vapor escape. Small-scale pores benefit the formation of water clusters containing several to dozens of water molecules during the solar steam generation process, which contributes to reducing the evaporation enthalpy.

Here, samples of 2 layers, 4 layers, 6 layers, 8 layers, 10 layers, 15 layers, 20 layers, and 25 layers assembled by cotton paper using the method described above were studied under the same experimental conditions. The ambient temperature and humidity were calibrated at 24 °C and 58%, respectively. Temperature changes of the evaporation surface, the distance of 5mm beneath the water surface, and the air gap were all recorded. The thermal behavior as shown in Fig. 4a, proved that the laser-transferred graphene has ideal photothermal conversion capability. All the samples were able to achieve a stable temperature around 40 °C in the initial 40 min under one sun intensity. For a fixed solar intensity, higher operation temperature typically indicates lower energy transfer efficiency. The evaporator with fewer layers of cotton paper showed the fastest heat response. A temperature as high as 41 °C stabilized within 17 min for the evaporators with no more than 6 layers. As the number of layers increased, the evaporator surface temperature showed a downward trend, which means an enhanced cooling effect caused by more intense evaporation behavior. The large difference between the temperature of the evaporator surface and the water body confirmed the adiabatic effect of the air gap, indicating its outstanding scalability for reducing the downward conduction heat losses.

At the end of the evaporation process, the water temperature had only risen by less than 4 °C. It is worth noticing that, since there were higher temperature rises in the test site close to the water surface, the underlying bulk water remained at a preferable lower temperature. Moreover, the hot end of the air layer was always on top while the cold end was always below, so the heat transfer mechanism here was mainly heat conduction. The humid air thermal conductivity of the mixture can be estimated as a function of mixture temperature with relative humidity [36, 37].

$$\lambda_{mixture} = \sum_{i=1}^{n} \frac{x_i \cdot \lambda_i}{\sum_{j=1}^{n} x_j A_{ij}} \quad (1)$$

where $\lambda_{mixture}$ represents the thermal conductivity of humid air (W m^{-1} k^{-1}), x and λ are defined as the molar fraction and the thermal conductivity of each component in the mixture, respectively. A_{ij} is the interaction parameter of the components. For this humid air system, there are only two components: water vapor and dry air, which are represented by "v" and "da" in the math formulae, respectively. For this humid air system, the interaction parameters between vapor and dry air are given respectively:

$$A_{da-v} = \frac{\left[1+\left(\frac{\mu_{da}}{\mu_v}\right)^{1/2}\cdot\left(\frac{M_v}{M_{da}}\right)^{1/4}\right]^2}{\left[8\left(1+\left(\frac{M_{da}}{M_v}\right)\right)\right]^{1/2}} \quad (2)$$

$$A_{v-da} = \frac{\mu_v}{\mu_{da}} \cdot \frac{M_{da}}{M_v} \cdot A_{da-v} \quad (3)$$

$$A_{da-da} = A_{v-v} = 1 \quad (4)$$

In Eq. (2) and Eq. (3), M_v is the equivalent molecular weight of water vapor, taking 28.97. M_{da} represents the equivalent molecular weight of dry air, taking 18.02. μ_v and μ_{da} in Ns m^{-1} are the corresponding viscosity of vapor and dry air, respectively.

The specific calculation process derived from Eq. (1) can be displayed as follows:

$$\lambda_{mixture} = \frac{x_{da} \cdot \lambda_{da}}{x_{da} + x_v \cdot A_{da-v}} + \frac{x_v \cdot \lambda_v}{x_v + x_{da} \cdot A_{v-da}} \quad (5)$$

When the temperature of the air layer is 30℃, λ_{da} and λ_v are 0.025 and 0.020 W m^{-1} k^{-1}, respectively. The molar fraction values of x_{da} and x_v in the previous expression are calculated by,

$$x_{da} = \frac{M_{mixture}}{M_{da}} a_{da} \quad (6)$$

$$x_v = \frac{M_{mixture}}{M_v} a_v \quad (7)$$

where, $M_{misture}$ is the equivalent molecular weight of wet air. a_{da} and a_v are the mass fraction of dry air and vapor in the system, respectively. q (Kg) represents the quality of water in wet air containing 1 kg of dry air.

$$\mathrm{q} = 0.622 \frac{RH\% \cdot P(T)}{P_0 - RH\% \cdot P(T)} \quad (8)$$

where $RH\%$ and P_0 (Pa) are the relative humidity and pressure of the environment (air gap layer in the steam generation experiment), respectively. And $P(T)$ (Pa) denotes the water vapor saturation pressure at a humid air temperature of T (℃). Then Eq. (5) can be simplified as Eq. (9).

$$\lambda_{mixture} = \frac{\lambda_{da}}{1 + q\frac{M_{da}}{M_v} A_{da-v}} + \frac{\lambda_v}{1 + q\frac{M_v}{M_{da}} A_{v-da}} \quad (9)$$

In the steady-state, the relative humidity and temperature in the closed test chamber were 95% RH and 31 °C, respectively. Based on Eq. (2-9), the theoretical thermal conductivity of the air gap layer during the operation was calculated to increase from 0.025 W m^{-1} K^{-1} to 0.027 W m^{-1} K^{-1} at the end of the experiment. Although the thermal conductivity slightly increases with temperature and humidity, it remains at a very favorable level.

Contributed by the high-water absorption and adequate micro capillary capacity, multilayer cotton paper forms a large volume 3D evaporator readily. When the number of layers increased from 2 to 25, the dark evaporation rate increased from 331 to 504 g m^{-2} h^{-1} because of the amplified evaporation area, as showed in Figure 3b. The evaporation component exhibited a temperature significantly lower than the underlying water, indicating the evaporative heat dissipation. The evaporation rate and corresponding energy conversation efficiency under one sun illumination are plotted in Figure 3c. When the total number of cotton paper layers is below 15, the evaporation rate gradually increases from 1183 to 1721 g m^{-2} h^{-1}. This enhancement is mainly due to the enlarged 3D structure and the increased amount of saturated water therein. For comparison, without processed-cotton paper as the photothermal conversion mediator and 3D structure amplifier, the evaporation rate of pure water is 360 g m^{-2} h^{-1}. However, with a further increase in layers, there is a slight downward trend in evaporation efficiency. Excessive water content sacrifices the solar energy and impedes timely and adequate heating of the solar interfacial evaporator. This is also the reason why the evaporation surface temperature drops when the number of layers is increased to a certain extent.

Evaporation efficiency η (%) is another important factor in evaluating the photothermal performance of 3D solar steam generation systems and can be calculated as:

$$\eta = \dot{m}h / C_{opt} P_0 \quad (10)$$

where $\dot{m}$ denotes the mass loss while reaching steady-state deducing dark field evaporation, h (kJ mol^{-1}) is the latent enthalpy of water vaporization, C_{opt} is the optical concentration (as for this work is free from optical accessories, so C_{opt} is equal to 1 here), p_0 refers to the solar irradiation intensity (1000 W m^{-2}). As shown in Fig. 3c, the η of the l0-layer sample was calculated to be 83%, demonstrating that the cotton paper-based 3D evaporator can achieve high solar illumination utilization. Further increase of the cotton paper layers impairs efficiency and it is mainly due to the boosted evaporation under darkfield conditions. It is deduced that a rapid decline in efficiency will be the result of a continued increase in the number of layers. Effective control of the number of layers is of great importance for the cost and assembly labor-saving in actual applications. Moreover, the stability of the 10-layer evaporator was investigated. Before testing, the sample was immersed in water for 12 hours. As shown in Fig. 5, the performance remains stable for 100 cycles, ensuring long-term stable water purification ability. Economic viability based on the evaporation performance and the cost is a vital consideration factor for real-world applications. According to a related research [38], a median intake of 3.7 liters of water satisfies one's daily freshwater consumption needs. Taking into account the changeable environmental factors, when the average operation period is 5 hours (from 10:00 am-3:00 pm) a day, only 0.45 m^2 of laser-processed 10-layer cotton paper is needed, and the retail cost at such amount is ~ US$ 5 in this experiment. Since more than 65 million tons of cotton fibers produced every year [39], the cost of cotton paper can be as low as ~ US$ 0.25 m^{-2} for bulk purchase (pricing data obtained from Alibaba.com), which is only one-third of the unit price of the cotton paper we purchased in this laboratory work. The estimated industrial mass-produced cotton paper-based steam generator costs $ 3.22 only with an area of 0.45 m^2. The specific cost estimation process is provided in Supplementary Information Note 2.1.

The simple solar still shown in Fig. 6a was used to perform the outdoor solar steam generation experiment on a partly sunny day with dramatically varying solar intensity (9 Jun 2019). Under natural sun conditions, an average evaporation rate of 720 g m^{-2} h^{-1} could be obtained. This difference from the laboratory-derived data was mainly due to the limited space that caused the sharply rising humidity in the whole solar still. The condensation of water droplets blurred the film and affects light transmission, which was also an important reason for the decrease in evaporation efficiency. A more optimized solar still device will get better results. As shown in Fig. 6b, the laser-processed cotton paper can be used for real-world applications, with a tailored laying area on the seawater surface. This configuration is more resistant to wind and waves and makes it easier for evaporator recycling as well as desalinated seawater collection. Besides, it is critical to understand the production cost associated with purified water. Water production

cost estimation of large scale solar still was also conducted according to the cost model and solar still developed by Cao.et al. [16] and Chen.et al. [40], respectively. Indicated by the cost accounting results reported in Ref. [16], the unit cost to produce clean water by solar steam generation ranged from US$ 0.007 L^{-1} to US$ 0.0675 L^{-1}. In contrast, our work's water production cost is only US$ 0.003 L^{-1}, showing a very superior cost-to-benefit ratio. The specific calculation process can be found in Supplementary Information Note 2.2. Moreover, the commonly used commercial desalination method is mainly reverse osmosis distillation, which suffers from high electricity consumption, complicated pretreatment procedures, and mass production of carbon dioxide. The solar energy-driven steam generation system is free from the dependence of electricity, further making it applicable in remote regions. Thus, our work provides the benefits of both low prices and high environmental friendliness.

Table 2 compares some of the water evaporation efficiencies and green index of recent reports focused on solar steam generation. Here, direct laser printing synthesis has a great advantage in green chemistry due to free from hazardous raw material involvement and additional waste generation. Although some evaporators based on carbonized biomass, such as logs [21, 41], mushrooms [42], daikon [43], and lotuses [44], are also environmentally friendly and raw materials used also cheap, the processing of these materials is difficult to get rid of the high-temperature treatment in a costly inert gas environment. The cost efficiencies of these methods are highly degraded by tedious processing procedures. Meanwhile, due to incompletely controllable shape and low decay resistance, their long-term evaporation performance and large-scale promotion in the oceans are limited. As a kind of naturally degradable crop product with minimal effect on the ecosystem, cotton paper can be obtained by simple weaving processes and is able to be freely tailored, suggesting that our approach has the merits in terms of abundance, non-toxicity, simple processing and high scalability.

Table 2. Comparison of evaporation performance under 1 sun and green index of different works

Work	**Evaporation efficiency ($kg\ m^{-2}\ h^{-1}$)**	**Efficiency**	**Free from chemicals**	**Free from waste generation**	**Free from special processing condition**	**Reference**
3D printing processed cotton-paper	1.71	83%	√	√	√	Our work

Au/Ag-cotton fibers	1.4	86.3%	√	√	×	[11]
Cotton-CuS	1.63	94.9	×	×	×	[45]
Carbonized mushroom	1.475	68%	√	√	×	[42]
Carbonized wood	1	~70%	√	√	×	[41]
Carbon lotus	1.3	86.5%	√	√	×	[44]
Surface-modified sponge	1.18	73.3%	×	×	×	[46]
Calcinated melamine sponges	1.98	92%	√	√	×	[28]
Multilayer Ppy nanosheets	1.38	95.33%	×	×	√	[4]
Carbon nanosheet frameworks	1.48	93%	×	×	×	[15]
PVA-Ppy gels	3.2	94	×	×	×	[47]
Surface tailored PVA hydrogel	2.6	91%	×	×	×	[48]
MOF derived porous carbon materials	1.22	84.3%	×	×	×	[49]
Au nanorods decorated GO	1.34	84.1%	×	×	√	[9]
Au@Bi_2MoO_6-CDs	1.69	97.1%	×	×	×	[10]

3. Conclusions

In summary, we have demonstrated a scalable and economical cotton paper-based 3D solar steam generator prepared by a laser-induced graphene transformation process in an ambient atmosphere. The novel one-step evaporator exhibits high light-trapping efficiency of 98.5% over a broad optical spectrum. Moreover, a new design using an air gap as the thermal insulator to suppress the heat conduction loss helps the multilayer cotton paper-based evaporator achieve a maximum evaporation rate of 1711 g m^{-2} h^{-1} with a corresponding efficiency of 83%. The thermal conductivity of the air gap layer can always be kept below 0.028 W m^{-1} K^{-1} during operation, even superior to many

plastic foams, such as nylon. To our best knowledge, these evaporation values outperform most of the solar-driven evaporators that have been reported without the application of artificial insulation material and optical accessories. Furthermore, this high efficiency and biodegradable laser-processed cotton paper evaporator is expected to provide a workable solution for solving the freshwater crisis in a greener chemistry approach. Our work also provides inspirations for the future development of high-performance solar-driven evaporators at a low cost.

CRediT authorship contribution statement

Y.L. Wang: Conceptualization, Methodology, Data curation, Writing - original draft, Writing - review & editing. G.J. Li: Conceptualization, Writing - review & editing. K.C. Chan: Supervision, Conceptualization, Writing - review & editing.

Declaration of Competing Interest

The authors declare that they have no known competing financial interests or personal relationships that could appear to influence the work reported in this paper.

Acknowledgment

This work was supported by the Faculty of Engineering of The Hong Kong Polytechnic University under the account no. 1-45-37-99QP.

Reference

[1] O. Ellabban, H. Abu-Rub, F. Blaabjerg, Renewable energy resources: Current status, future prospects and their enabling technology, Renew. Sust. Energ. Rev. 39 (2014) 748-764, https://doi.org/10.1016/j.rser.2014.07.113.
[2] P. Tao, G. Ni, C. Song, W. Shang, J. Wu, J. Zhu, G. Chen, T. Deng, Solar-driven interfacial evaporation, Nat. Energy 3 (2018) 1031-1041, http://dx.doi.org/10.1038/s41560-018-0260-7.

[3] Q. Wang, Z. Zhu, G. Wu, X. Zhang, H. Zheng, Energy analysis and experimental verification of a solar freshwater self-produced ecological film floating on the sea, Appl. Energy 224 (2018) 510-526, http://dx.doi.org/10.1016/j.apenergy.2018.05.010.
[4] X. Wang, Q. Liu, S. Wu, B. Xu, H. Xu, Multilayer polypyrrole nanosheets with self−organized surface structures for flexible and efficient solar-thermal energy conversion, Adv. Mater. 31 (2019) 1807716, http://dx.doi.org/10.1002/adma.201807716.
[5] H. Ghasemi, G. Ni, A.M. Marconnet, J. Loomis, S. Yerci, N. Miljkovic, G. Chen, Solar steam generation by heat localization, Nat. Commun. 5 (2014) 4449, http://dx.doi.org/10.1038/ncomms5449.
[6] C. Chang, C. Yang, Y. Liu, P. Tao, C. Song, W. Shang, J. Wu, T. Deng, Efficient solar-thermal energy harvest driven by interfacial plasmonic heating-assisted evaporation, ACS Appl. Mater. Interfaces 8 (2016) 23412-23418, http://dx.doi.org/10.1021/acsami.6b08077.
[7] Z. Deng, J. Zhou, L. Miao, C. Liu, Y. Peng, L. Sun, S. Tanemura, The emergence of solar thermal utilization: solar-driven steam generation, J. Mater. Chem. A 5 (2017) 7691-7709, http://dx.doi.org/10.1039/C7TA01361B.
[8] H.D. Kiriarachchi, F.S. Awad, A.A. Hassan, J.A. Bobb, A. Lin, M.S. El-Shall, Plasmonic chemically modified cotton nanocomposite fibers for efficient solar water desalination and wastewater treatment, Nanoscale, 10 (2018) 18531-18539, http://dx.doi.org/10.1039/C8NR05916K.
[9] J. Zhou, Y. Gu, Z. Deng, L. Miao, H. Su, P. Wang, J. Shi, The dispersion of Au nanorods decorated on graphene oxide nanosheets for solar steam generation, Sustain. Mater. Technol. 19 (2019) e00090, http://dx.doi.org/10.1016/j.susmat.2018.e00090.
[10] Z. Zheng, H. Li, X. Zhang, H. Jiang, X. Geng, S. Li, H. Tu, X. Cheng, P. Yang, Y. Wan, High-absorption solar steam device comprising Au@ Bi_2MoO_6-CDs: extraordinary desalination and electricity generation, Nano Energy 68 (2020) 104298, http://dx.doi.org/10.1016/j.nanoen.2019.104298.
[11] Q. Zhu, K. Ye, W. Zhu, W. Xu, C. Zou, L. Song, E. Sharman, L. Wang, S. Jin, G. Zhang, A Hydrogenated Metal-Oxide with Full Solar Spectrum Absorption for Highly Efficient Photothermal Water Evaporation, J. Phys. Chem. Lett (2020), http://dx.doi.org/10.1021/acs.jpclett.0c00592.
[12] Z. Zhang, Y. Wang, P.A.S. Hansen, K. Du, K.R. Gustavsen, G. Liu, F. Karlsen, O. Nilsen, C. Xue, K. Wang, Black silicon with order-disordered structures for enhanced light trapping and photothermic conversion, Nano Energy, 65 (2019) 103992, http://dx.doi.org/10.1016/j.nanoen.2019.103992.
[13] Z. Li, M. Zheng, N. Wei, Y. Lin, W. Chu, R. Xu, H. Wang, J. Tian, H. Cui, Broadband-absorbing WO_{3-x} nanorod-decorated wood evaporator for highly efficient solar-driven interfacial steam generation, Sol. Energy Mater. Sol. Cells 205 (2020) 110254, http://dx.doi.org/10.1016/j.solmat.2019.110254.
[14] A. Abbas, Y. Zhao, J. Zhou, X. Wang, T. Lin, Improving thermal conductivity of cotton fabrics using composite coatings containing graphene, multiwall carbon nanotube or boron nitride fine particles, Fibers Polym. 14 (2013) 1641-1649, http://dx.doi.org/10.1007/s12221-013-1641-y.
[15] L. Sun, J. Liu, Y. Zhao, J. Xu, Y. Li, Highly efficient solar steam generation via mass-produced carbon nanosheet frameworks, Carbon, 145 (2019) 352-358, http://dx.doi.org/10.1016/j.carbon.2019.01.040.
[16] S. Cao, Q. Jiang, X. Wu, D. Ghim, H.G. Derami, P.-I. Chou, Y.-S. Jun, S. Singamaneni, Advances in solar evaporator materials for freshwater generation, J. Mater. Chem. A 7 (2019) 24092-24123, http://dx.doi.org/10.1039/C9TA06034K.
[17] C. Liu, J. Huang, C.E. Hsiung, Y. Tian, J. Wang, Y. Han, A. Fratalocchi, Solar Steam Generation: High−Performance Large−Scale Solar Steam Generation with Nanolayers of Reusable Biomimetic Nanoparticles, Adv. Sustainable Syst. 1 (2017) 1600013, http://dx.doi.org/10.1002/adsu.201600013.
[18] M. Zhu, Y. Li, F. Chen, X. Zhu, J. Dai, Y. Li, Z. Yang, X. Yan, J. Song, Y. Wang, Plasmonic wood for high−efficiency solar steam generation, Adv. Energy Mater. 8 (2018) 1701028, http://dx.doi.org/10.1002/aenm.201701028.
[19] M. Ye, J. Jia, Z. Wu, C. Qian, R. Chen, P.G. O'Brien, W. Sun, Y. Dong, G.A. Ozin, Synthesis of black TiO_x nanoparticles by Mg reduction of TiO_2 nanocrystals and their application for solar water evaporation, Adv. Energy Mater. 7 (2017) 1601811, https://doi.org/10.1002/aenm.201601811.

[20] Q. Jiang, L. Tian, K.K. Liu, S. Tadepalli, R. Raliya, P. Biswas, R.R. Naik, S. Singamaneni, Bilayered biofoam for highly efficient solar steam generation, Adv. Mater. 28 (2016) 9400-9407, http://dx.doi.org/10.1002/adma.201601819.
[21] G. Xue, K. Liu, Q. Chen, P. Yang, J. Li, T. Ding, J. Duan, B. Qi, J. Zhou, Robust and low-cost flame-treated wood for high-performance solar steam generation, ACS Appl. Mater. Interfaces 9 (2017) 15052-15057, http://dx.doi.org/10.1021/acsami.7b01992.
[22] G. Zhu, J. Xu, W. Zhao, F. Huang, Constructing black titania with unique nanocage structure for solar desalination, ACS Appl. Mater. Interfaces 8 (2016) 31716-31721, http://dx.doi.org/10.1021/acsami.6b11466.
[23] X. Li, W. Xu, M. Tang, L. Zhou, B. Zhu, S. Zhu, J. Zhu, Graphene oxide-based efficient and scalable solar desalination under one sun with a confined 2D water path, PNAS 113 (2016) 13953-13958, http://dx.doi.org/10.1073/pnas.1613031113.
[24] L. Cui, P. Zhang, Y. Xiao, Y. Liang, H. Liang, Z. Cheng, L. Qu, High Rate Production of Clean Water Based on the Combined Photo-Electro-Thermal Effect of Graphene Architecture, Adv. Mater. 30 (2018) 1706805, http://dx.doi.org/10.1002/adma.201706805.
[25] J. Li, M. Du, G. Lv, L. Zhou, X. Li, L. Bertoluzzi, C. Liu, S. Zhu, J. Zhu, Interfacial solar steam generation enables fast−responsive, energy−efficient, and low−cost off−grid sterilization, Adv. Mater. 30 (2018) 1805159, http://dx.doi.org/10.1002/adma.201805159.
[26] L. Zhou, X. Li, G.W. Ni, S. Zhu, J. Zhu, The revival of thermal utilization from the Sun: interfacial solar vapor generation, Natl. Sci. Rev. 6 (2019) 562-578, http://dx.doi.org/10.1093/nsr/nwz030.
[27] G. Ni, G. Li, S.V. Boriskina, H. Li, W. Yang, T. Zhang, G. Chen, Steam generation under one sun enabled by a floating structure with thermal concentration, Nat. Energy 1 (2016) 1-7, http://dx.doi.org/10.1038/nenergy.2016.126.
[28] F.F. Gong, H. Li, W. Wang, J. Huang, D.D. Xia, J. Liao, M. Wu, D.V. Papavassiliou, Scalable, eco-friendly and ultrafast solar steam generators based on one-step melamine-derived carbon sponges toward water purification, Nano Energy, 58 (2019) 322-330, http://dx.doi.org/10.1016/j.nanoen.2019.01.044.
[29] Q. Ding, C. Guan, H. Li, M. Shi, W. Yang, H. Yan, X. Zuo, Y. An, S. Ramakrishna, P. Mohankumar, Solar-driven interfacial evaporation based on double-layer polylactic acid fibrous membranes loading Chinese ink nanoparticles, Sol. Energy 195 (2020) 636-643, https://doi.org/10.1016/j.solener.2019.11.078.
[30] Y. Yang, W. Que, J. Zhao, Y. Han, M. Ju, X. Yin, Membrane assembled from anti-fouling copper-zinc-tin-selenide nanocarambolas for solar-driven interfacial water evaporation, Chem. Eng. J. 373 (2019) 955-962, http://dx.doi.org/10.1016/j.cej.2019.05.099.
[31] H.M. Wilson, S.R. AR, A.E. Parab, N. Jha, Ultra-low cost cotton based solar evaporation device for seawater desalination and waste water purification to produce drinkable water, Desalination, 456 (2019) 85-96, http://dx.doi.org/10.1016/j.desal.2019.01.017.
[32] K. Yin, S. Yang, J. Wu, Y. Li, D. Chu, J. He, J. A. Duan, Femtosecond laser induced robust Ti foam based evaporator for efficient solar desalination, J. Mater. Chem. A 7 (2019) 8361-8367, http://dx.doi.org/10.1039/C9TA00291J.
[33] N. Jiang, Y. Wang, K.C. Chan, C.Y. Chan, H. Sun, G. Li, Additive manufactured graphene coating with synergistic photothermal and superhydrophobic effects for bactericidal applications, Glob. Chall. 4 (2020) 1900054, http://dx.doi.org/10.1002/gch2.201900054.
[34] G. Li, X. Mo, Y. Wang, C.Y. Chan, K.C. Chan, All 3D−printed superhydrophobic/oleophilic membrane for robotic oil recycling, Adv. Mater. Interfaces 6 (2019) 1900874, http://dx.doi.org/10.1002/admi.201900874.
[35] G. Li, W.C. Law, K.C. Chan, Floating, highly efficient, and scalable graphene membranes for seawater desalination using solar energy, Green Chem. 20 (2018) 3689-3695, http://dx.doi.org/10.1039/C8GC01347K.

[36] P. Tsilingiris, Thermophysical and transport properties of humid air at temperature range between 0 and 100 °C, Energy Convers. Manag. 49 (2008) 1098-1110, https://doi.org/10.1016/j.enconman.2007.09.015.
[37] R.C. Reid, J.M. Prausnitz, B.E. Poling, The properties of gases and liquids, (1987).
[38] M.N. Sawka, S.N. Cheuvront, R. Carter, Human water needs, Nutr. Rev. 63 (2005) S30-S39, https://doi.org/10.1111/j.1753-4887.2005.tb00152.x.
[39] K. Jabran, B.S. Chauhan, Cotton Production, John Wiley & Sons, 2019.
[40] T.A. Cooper, S.H. Zandavi, G.W. Ni, Y. Tsurimaki, Y. Huang, S.V. Boriskina, G. Chen, Contactless steam generation and superheating under one sun illumination, Nat. Commun. 9 (2018) 1-10, http://dx.doi.org/10.1038/s41467-018-07494-2.
[41] M. Zhu, Y. Li, G. Chen, F. Jiang, Z. Yang, X. Luo, Y. Wang, S.D. Lacey, J. Dai, C. Wang, Tree-inspired design for high-efficiency water extraction, Adv. Mater. 29 (2017) 1704107, http://dx.doi.org/10.1002/adma.201704107.
[42] N. Xu, X. Hu, W. Xu, X. Li, L. Zhou, S. Zhu, J. Zhu, Mushrooms as efficient solar steam-generation devices, Adv. Mater. 29 (2017) 1606762, http://dx.doi.org/10.1002/adma.201606762.
[43] M. Zhu, J. Yu, C. Ma, C. Zhang, D. Wu, H. Zhu, Carbonized daikon for high efficient solar steam generation, Sol. Energy Mater Sol. Cells 191 (2019) 83-90, http://dx.doi.org/10.1016/j.solmat.2018.11.015.
[44] J. Fang, J. Liu, J. Gu, Q. Liu, W. Zhang, H. Su, D. Zhang, Hierarchical porous carbonized lotus seedpods for highly efficient solar steam generation, Chem. Mater. 30 (2018) 6217-6221, http://dx.doi.org/10.1021/acs.chemmater.8b01702.
[45] X. Wu, M.E. Robson, J.L. Phelps, J.S. Tan, B. Shao, G. Owens, H. Xu, A flexible photothermal cotton-CuS nanocage-agarose aerogel towards portable solar steam generation, Nano energy 56 (2019) 708-715, http://dx.doi.org/10.1016/j.nanoen.2018.12.008.
[46] Z. Zhang, P. Mu, J. He, Z. Zhu, H. Sun, H. Wei, W. Liang, A. Li, Facile and scalable fabrication of surface−modified sponge for efficient solar steam generation, ChemSusChem 12 (2019) 426-433, http://dx.doi.org/10.1002/cssc.201802406.
[47] F. Zhao, X. Zhou, Y. Shi, X. Qian, M. Alexander, X. Zhao, S. Mendez, R. Yang, L. Qu, G. Yu, Highly efficient solar vapour generation via hierarchically nanostructured gels, Nat. Nanotechnol. 13 (2018) 489-495, http://dx.doi.org/10.1038/s41565-018-0097-z.
[48] Y. Guo, F. Zhao, X. Zhou, Z. Chen, G. Yu, Tailoring nanoscale surface topography of hydrogel for efficient solar vapor generation, Nano Lett. 19 (2019) 2530-2536, http://dx.doi.org/10.1021/acs.nanolett.9b00252.
[49] S. Ma, W. Qarony, M.I. Hossain, C.T. Yip, Y.H. Tsang, Metal-organic framework derived porous carbon of light trapping structures for efficient solar steam generation, Sol. Energy Mater Sol. Cells 196 (2019) 36-42, http://dx.doi.org/10.1016/j.solmat.2019.02.035.

Figure captions

Fig. 1 Design of cotton paper-based 3D solar vapor generation device. (a)Schematic illustration of using plastic foam as a thermal insulator. (b)Schematic illustration of using an air gap as a thermal insulator. (c) Laser processing process (d) Assembly process of multilayer evaporator.

Fig. 2 Characterization of cotton paper before and after laser processing. (a) Raman spectra of the processed cotton paper. (b) UV-vis absorption spectra of cotton paper before and after graphene-deposited.

Fig. 3 Microstructures observation of cotton paper before and after laser processing. (a) SEM image of the untreated cotton paper. (b) Zoom-in SEM image of the untreated cotton paper. (c) SEM image of the laser-treated cotton paper. (d) Zoom-in SEM image of the laser-treated cotton paper.

Fig. 4 Solar evaporation performance of cotton paper-based evaporator. (a) Schematic illustration of photothermal conversion capability of the evaporator. (b) Saturated water weight and dark evaporation rate of multilayer evaporator. (c) Evaporation rate under one sun illumination. (d) Evaporation efficiency under one sun illumination.

Fig. 5 Long-term evaporation cycle performance of the 10-layer evaporator.

Fig. 6 (a) Photo of solar still used in the outdoor experiment. (b)Schematic illustration for a real-world application example of the cotton paper-based steam generator on the coast.

Fig.1

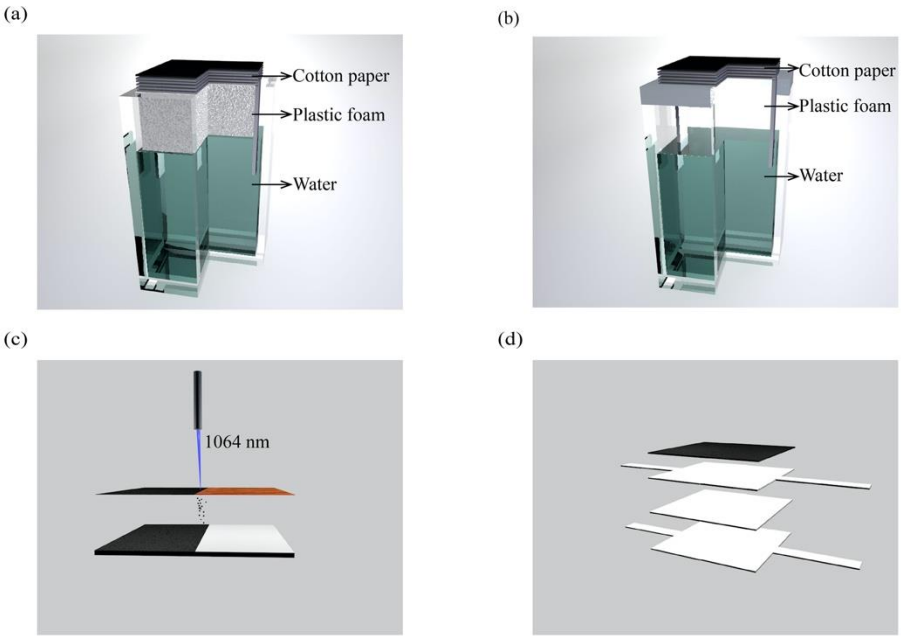
(a)
Cotton paper
Plastic foam
Water
(b)
Cotton paper
Plastic foam
Water
(c)
1064 nm
(d)

Fig.2

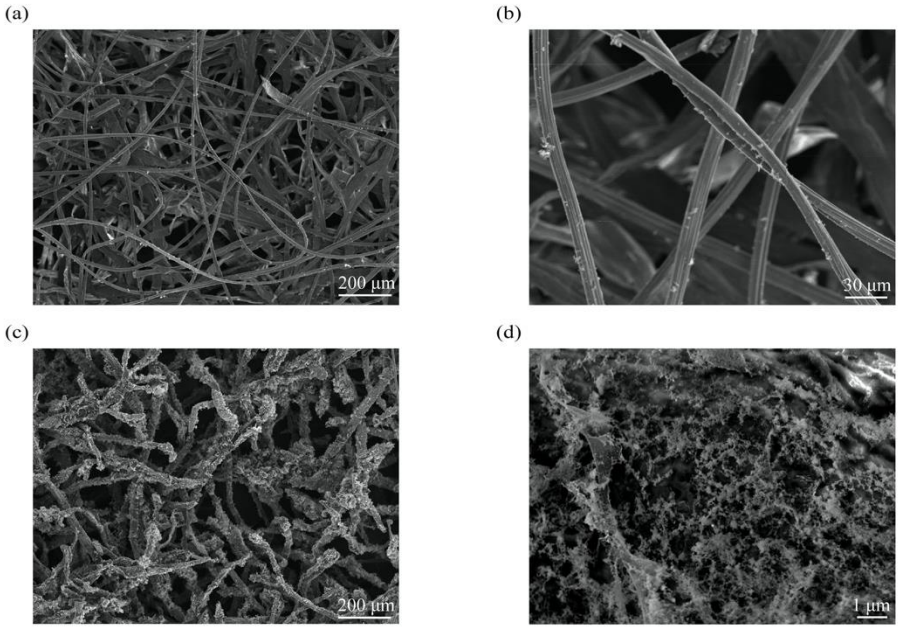
(a)
200 μm
(b)
30 μm
(c)
200 μm
(d)
1 μm

Fig.3

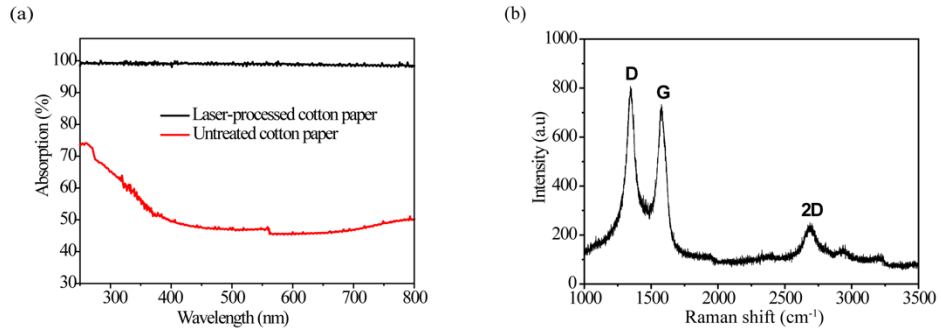
(a)
Absorption (%)
Wavelength (nm)
Laser-processed cotton paper
Untreated cotton paper
(b)
Intensity (a.u)
Raman shift (cm-1)
D
G
2D

Fig.4

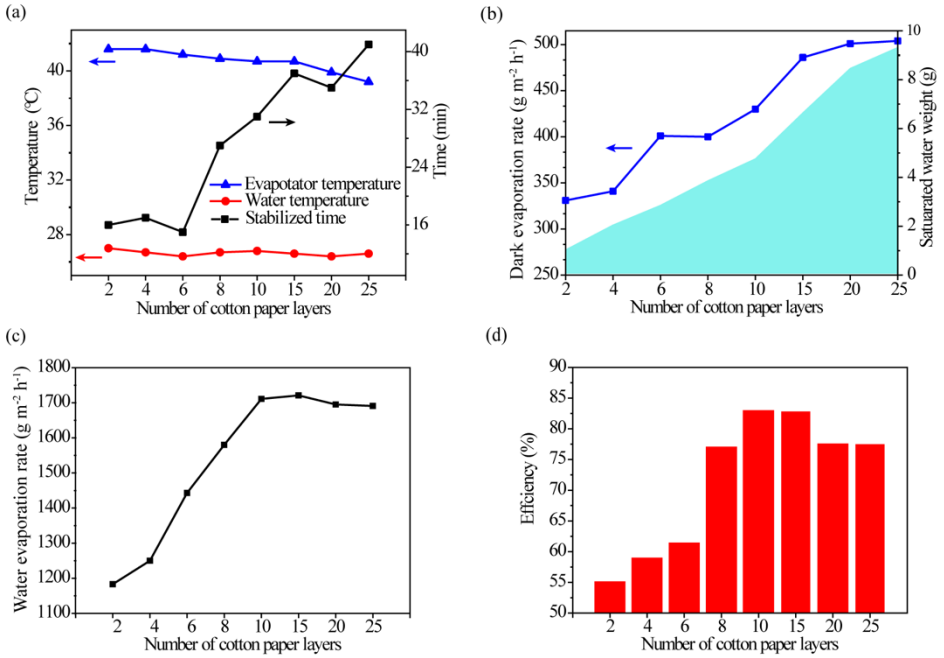
(a)
Temperature (℃)
Time (min)
Evapotator temperature
Water temperature
Stabilized time
Number of cotton paper layers
(b)
Dark evaporation rate (g m-2 h-1)
Satuarated water weight (g)
Number of cotton paper layers
(c)
Water evaporation rate (g m-2 h-1)
Number of cotton paper layers
(d)
Efficiency (%)
Number of cotton paper layers

Fig.5

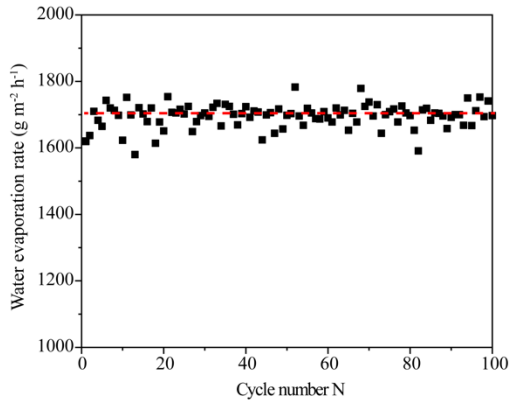
Water evaporation rate (g m^{-2} h^{-1})
2000
1800
1600
1400
1200
1000
0
20
40
60
80
100
Cycle number N

Fig.6

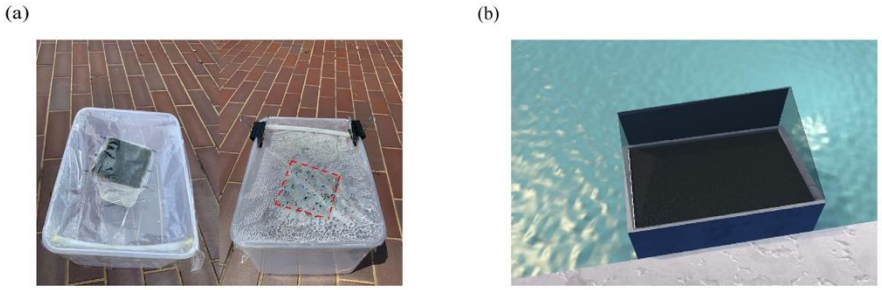
(a)
(b)